Proceedings of the Fourth Lunar Science Conference
(Supplement 4, *Geochimica et Cosmochimica Acta*)
Vol. 3, pp. 3255–3276

Crater populations on lunar rocks

GERHARD NEUKUM*

Lunar Science Institute, Houston, Texas 77058

FRIEDRICH HÖRZ and DONALD A. MORRISON

NASA Johnson Space Center, Houston, Texas 77058

JACK B. HARTUNG

Max-Planck-Institut für Kernphysik, Heidelberg, Germany

Abstract—Approximately 10,000 microcraters were investigated using binocular microscope techniques on fifteen Apollo 16 rocks: "crystalline" rocks 60315, 60335, 61156, 62235, 62295, and 68415; "breccias" 60016, 61015, 61175, 66075, and 69935; and glass surfaces 60015, 60095, 60135, and 64455. Diameter measurements of the central glass-lined pits (D_P) and surrounding spall zones (D_S) were made. Ratios of spall to pit diameters may range from 3.0 to 4.5 for different rock surfaces.

Crater size distributions obtained for production surfaces confirm and extend to larger crater sizes data published previously. The crater size distribution on lunar rocks in the pit diameter range, 10 to 1000 microns, is shown to depend on the average angle of impact which is a function of the exposure geometry.

In contrast to results of earlier studies, a wide range of crater densities was observed on relatively heavily cratered surfaces. The highest crater densities observed for lunar breccias are about a factor of 2 higher than that for crystalline rocks, which, in turn, appear up to 4 times more densely cratered than loose regolith in equilibrium.

Analytical models yield the expression for the cumulative equilibrium crater density, $N_E = AD_S^{-2}$, which has been adapted to microcratering on lunar rocks. A minimum value for the coefficient, A, is 0.15 assuming the largest measured spall-to-pit-diameter ratio of 4.5. This minimum is consistent with measurements.

Four independent criteria for recognizing equilibrium populations, (1) absolute crater densities, (2) constant crater densities for different exposure angles, (3) extent of D^{-2} slope, and (4) erosional state of surface, were applied to nine non-production Apollo 16 rocks, but only populations from two rocks (62235, 66075) satisfied all four criteria and were unambiguously shown to be in an equilibrium state.

INTRODUCTION

INVESTIGATION of impact craters caused by primary micrometeoroids on returned lunar materials is of interest for a variety of lunar studies. Such investigations may yield the flux of particulate interplanetary matter in the 10^{-5} to 10^{-15} g mass range in near lunar space (Neukum *et al.*, 1972; Morrison *et al.*, 1972; Hartung *et al.*, 1972; Schneider *et al.*, 1972) and also contribute to an improved understanding of small scale lunar surface processes, such as ionization, vaporization, melting, erosion, and transport—laterally and vertically—of regolith materials (Gault *et al.*,

*Permanent address: Max-Planck-Institut für Kernphysik, Heidelberg, Germany.

1972). At present these processes are understood only in a rather qualitative manner because the mass distribution and flux of meteoritic material over geologic times are not known accurately. The purpose of this paper is to describe and discuss the significance of microcrater populations on a variety of Apollo 16 rocks. Detailed models of meteoroid mass distributions and fluxes will be presented in subsequent papers together with implications for small scale lunar surface processes and exposure age information.

Two major objectives were pursued in these studies. The first objective was to determine the size distribution of crater populations in the "production" state (Shoemaker *et al.*, 1969; Gault, 1970) and thereby improve our knowledge about the mass distribution of micrometeoroids. This first objective requires rock surfaces of low absolute crater density.

In contrast, the second objective was to characterize crater size distributions typical of the highest observable crater densities on individual rock surfaces, i.e., those in or approaching equilibrium with respect to the cratering process (Shoemaker *et al.*, 1970; Gault, 1970). These investigations were stimulated by a systematic difference in absolute crater density between Apollo 12 basaltic rocks (Hörz *et al.*, 1971) and Apollo 14 breccias (Morrison *et al.*, 1972). The highest crater densities measured on Apollo 12 rocks are approximately a factor of 3 lower than the highest values observed on Apollo 14 breccias. Consequently, a variety of Apollo 16 crystalline rocks and breccias with high crater densities were investigated. An understanding of these highest crater densities is paramount to the interpretation of exposure histories as well as erosion mechanisms and rates on whole lunar rocks.

OBSERVATIONAL PROCEDURES

A total of fifteen Apollo 16 rocks were investigated, the selection criteria being to obtain a variety of rock types and a variety of crater densities as judged with the naked eye, according to the two main objectives outlined above. The following rocks were selected: glass surfaces: 60015, 60095, 60135, 64455; "crystalline" rocks: 60315, 60335, 61156, 62235, 62295, 68415; "breccias": 60016, 61015, 61175, 66075, 69935. For this discussion "crystalline" is defined to include truly igneous and high grade metamorphic rocks; "breccias" include both polymict clastic as well as partially molten breccias. This division may be greatly over-simplified and is subject to revision as detailed petrographic and, most importantly, data on physical properties governing the process of crater formation become available. Pertinent data on these rocks are summarized in Table 1.

The rocks selected were studied with a binocular microscope in a similar fashion as described by Hörz *et al.* (1971), and Morrison *et al.* (1972). The lowest magnification used was 4×, the highest magnification was 40×. Under the microscope a crater was identified by the presence of a glass-lined central pit. The diameter, D_P, of each pit observed was recorded.

Because the spall zone surrounding a central pit is eroded and degraded in more than 80% of all cases, the measurement of the spall zone diameter, D_S, was confined in this study to very fresh craters. Morrison *et al.* (1972) found that the ratio D_S/D_P varies significantly with rock types. Because the effective crater diameter is that of the spall zone rather than the pit, a precise characterization of D_S/D_P is necessary in order to convert the measured pit diameters of older craters, without recognizable spall zones, into spall diameters. Consequently, emphasis was placed on obtaining accurate D_S/D_P values on a given rock.

A variety of impact features were of the "pitless" crater type (McKay, 1970). Hartung *et al.* (1972) presented observational evidence suggestive of their origin by primary micrometeoroids. The total

Table 1. Summary of PET descriptions of rocks used in this study.

Rock	Rock Type[a]	Mass[b] (g)	Coherence[a]	Mode[c] (%) Opx	Opx	Plag	Ol.	Glass	Aphanitic	Size[d] (mm)	Surface[e] History
61156	III	58	2	18	—	65	12	—	—	—	Complex
60315	III	788	2	55	20	15	5	—	—	0.1	Simple†
68415	III	371	2	—	15.2	80	5	—	—	0.1	Simple‡
60335	III	318	2	—	—	70	25	3	—	0.1	
62235	III	320	2	45	—	45	—	—	—	1.0	Simple†
62295	III	251	2	24	—	57	—	—	16	0.4	Simple†
69935	IV	128	2	—	—	15	—	××	××		Simple‡
61015	IV	1803	2	—	40	55	—	—	—	0.2	?
61175	I	543	1	—	15	80	—	—	—	—	?
66075	I	347	2	—	—	—	—	—	××	0.1	Simple†
60016	I	4307	1	—	50	45	—	—	—	0.5	Complex†
60095	V	46	2	—	—	—	—	97	—	—	Complex
60015	II	5574	2	—	—	—	—	100*	—	—	Complex
60135	II	138	2	—	—	—	—	100*	—	—	Simple
64455	II	57	2	—	—	—	—	100*	—	—	Simple†

*Large glass coatings.

†Good lunar surface documentation.

‡Excellent lunar surface documentation.

[a]Classification according to LSPET (1972). Type I: Polymict breccia with clastic matrix. Type II: Cataclastic anorthosite. Type III: Igneous and high grade metamorphic rocks. Type IV: Partially molten breccias. Type V: Genuine glass.

[b]According to Lunar Sample Information Catalog, Apollo 16 (1972). (1) Friable. (2) Tough.

[c]According to LSPET (1972) Thin Section Descriptions. Mode of breccias refers to matrix only. (Opx = orthopyroxene, Cpx = clinopyroxene, Plag = plagioclase, Ol = olivine, × × present).

[d]Average grain size according to PET descriptions. There are significant ranges of grain sizes in individual samples.

[e]According to microcrater distributions (Hörz *et al.*, 1972). Complex: Tumbled repeatedly. Simple: Did not tumble; has uncratered surfaces.

abundance of these features generally is less than 5% of all impact craters. Some few rocks (e.g., 60015), however, displayed up to 20% pitless craters for the largest sizes. If such abundances occurred, the pitless crater diameters, i.e., the effective spall zones were measured and original diameters reconstructed via the measured D_S/D_P relationship.

Another phenomenon primarily observed on crystalline surfaces was the occurrence of large "halo" zones. Material was spalled off and the lighter microfractured underlying rock was easily visible. Because these zones could not be related to single impacts, we excluded these areas in the data reductions if more than 5% of the area of a field of view was so occupied.

The data reduction was identical to our previous studies. Only those fields of view which were representative of individual faces of a given rock, i.e., of similar geometry, were combined. Each individual surface investigated approximately represents the surface visible in the orthogonal photos obtained in the Lunar Receiving Laboratory (LRL) during the Preliminary Examination period. The "location" of a particular surface is described by the letters, T, B, N, S, E, and W, which correspond to similar indicators in these photos.

RESULTS

The detailed pit counts obtained at various magnifications are listed in Table 2 together with the total surface area observed at a given magnification. The specific location of this area with reference to a rock face shown in the LRL orthogonal photography is also given. The resulting cumulative size distributions are illustrated in Figs. 1 through 5. Both actual pit diameter distributions and the corresponding spall diameter distributions are shown. Collectively, a total of about 10,000 microcraters was counted.

Uncertainties in these data arise from a variety of sources. A comparison was made of the counting of different observers. An example of the agreement between two individuals is illustrated in Fig. 6. In general, the differences between observers was less than 20%, not including counts of the smaller craters. The statistical or counting uncertainties are indicated for each individual surface with error bars based on the square root of the sum of all craters larger than a given diameter. Other uncertainties are related to the selection and measurement of the areas studied, to the pit diameter measurement itself, and to the D_S/D_P determinations. These uncertainties refer to only the observed number of craters per unit area. Additional factors, such as some irregular spallation or a significant number of unobserved pitless craters, are difficult to evaluate. A conservative or high estimate, however, of the over-all uncertainty in the data presented is 50%.

INTERPRETATION

Production populations

A production surface is defined by a population of craters where destruction of pre-existing craters by subsequent impacts can be excluded. Therefore, they are of significant interest because size distribution of such a crater population directly reflects the energy distribution of the impacting micrometeoroids. Assuming certain standard velocities and densities for these micrometeoroids, these crater diameters eventually may be converted via empirical impact experiments into projectile masses and thereby into mass distributions of micrometeoroids.

Table 2. Cumulative frequencies of pit diameters at various magnifications on Apollo 16 rocks (μm).

Rock	Location	D_S/D_P	4× Magnification 500	750	100	1250	1500	1750	2000	2250	2500	2750	3000	3250	3500	3750[b]	(cm^2)[c]
60016	N	3.4	—	155	80	45	25	13	7	6	5	4	4	3	3	2	39.27
60315	T_1[d]	3.7	—	46	22	14	8	4									39.27
600315	T_1[d]	3.7	46	22	13	8	5	2	2	2	1	1	1				19.64
			5× Magnification 600	800	1000	1200	1400	1600									
69935	T	3.3	86	40	16	3	1	1									25.13
			8× Magnification 250	375	500	625	750	875	1000	1125	1250	1375	1500	1625	1750	1875	2000[b]	
60015	N	3.4	75	32	15	5												12.76
60016	N	3.4	—	211	129	87	50	36	23	17								14.73
60315	T_2	3.7	56	28	14	5	4											7.85
61015	T	3.3	—	235	124	66	28	22	10									14.73
61015	E	3.3	—	294	163	93	58	39	23	19	16	13	12	8				19.63
61175	T	3.0	—	319	196	148	89	59	38	19	18	6	6	2	2	2	2	14.73
62235	B	4.2	—	94	45	24	15	12	9	8	7	2	2	2	2	2	2	15.71
62235	W	4.2	114	76	30	13	6	3	1									9.82
62295	B	4.5	—	73	34	19	9	7	7	4	3							8.34
62295	S	4.5	—	20	8	6	3	1										4.91
68415	S	3.9	59	29	8	4												4.91
68415	N	3.9	299	162	59	24	11											24.54
69935	T	3.3	352	196	85	42	24	14	6									14.73
			10× Magnification 200	300	400	500	600	700	800	900	1000	1100	1200	1360	1400	1500	1600[b]	
60016	N	3.4	47	44	40	36	17	13	11	9	5	4						3.14
66075	T	3.4	—	293	203	147	95	71	51	33	27	15	11	6	4	4	2	11.94
66075	N	3.4	—	240	183	135	92	71	53	40	33	21	17	11	7	7	2	11.31
66075	S	3.4	—	159	108	74	47	37	30	22	16	11	10	8	7	5	2	6.28
66075	E	3.4	—	134	93	66	45	34	24	17	12	7	5	4	3	3	3	6.28
68415	S	3.9	65	30	18	10	4											4.58

Table 2. (continued)

Rock	Location	D_S/D_P	16× Magnification									(cm^2)[c]
			62.5	125	187.5	250	312.5	375	437.5	500[b]		
61156	E	4.4	69	38	16	7	4					3.18
61156	W	4.4	65	42	18	8	4					0.98
61156	T	4.4	—	96	90	56	32	16	9	1		3.82
61156	S	4.4	234	97	42	19	12	6	5	3		5.00

			20×Magnification																				
			50	100	150	200	250	300	350	400	450	500	550	600	650	700	750	800	850	900	950	>1000[b]	
60015	A[a]	3.4	—	318	176	103	65	36	23	12	10	7											7.62
60016	N	3.4	—	—	114	81	69	43	29	18													1.57
60095	A[a]	3.4	37	22	14	6	4																0.39
60315	T_2	3.7	—	73	47	25	17	8	6	4	4	3	2	2	2	1							1.57
60315	T_1	3.7	78	71	48	38	26	16	12	9	7	5	2	1									0.78
61015	T	3.3	—	—	282	174	129	82	62	46													3.14
61015	E	3.3	—	—	263	174	122	84	65	46	39												3.14
61175	T	3.0	—	—	—	111	85	64	56	46													2.36
62235	B	4.2	—	—	—	155	111	78	61	44	37	34	15										6.36
62235	W	4.2	—	138	99	67	47	32	21	10	8	7	2										2.36
62295	B	4.5	—	—	126	78	54	32	23	16	14	14	5										2.36
62295	S	4.5	—	—	22	14	10	7	4	4	3	3	1										0.78
64455	B	3.7	173	130	85	57	42	27	20	12	8	4	3	2	1	1							2.83
66075	T	3.4	—	—	143	104	85	59	42	30	27	23	15										1.57
66075	W	3.4	—	—	—	86	74	65	52	43	39	32	23	21	16	13	8						
68415	S	3.9	—	105	67	35	20	13															1.33
68415	N	3.9	—	246	172	106	77	48	30														3.93
69935	T_F	3.3	165	63	35	20	11	8	5	4	3	2	2	1									1.42
69935	T	3.3	—	631	407	257	179	109	83	60	47												4.71

			40× Magnification																					
			25	50	75	100	125	150	175	200	225	250	275	300	325	350	375	400	425	450	475	500	525	500[b]
60015	A[a]	3.4	—	457	305	210	161	117	85	59	45	33												3.93
60095	A[a]	3.4	53	40	21	14	9	7	4															0.70
60135	A[a]	3.4	—	351	231	138	92	62	40	23	15	8	4	1	1	1	1							1.37
60315	T_2	3.7	—	70	48	35	31	24	18	16	12	11												0.59
61015	T	3.3	—	—	250	180	153	125	104	81	64	58	38	37	31									1.37
61015	E	3.3	—	—	65	52	42	36	29															0.39
61156	N	4.4	25	21	13	9	6	4	1															2.23
62235	B	4.2	—	—	148	110	92	69	51	39	33	33	24	22	16									1.31
62235	W	4.2	—	81	60	39	35	25	19	13	12	12	9	8	5									0.59

62295	B	4.5	—	—	97	57	44	28	20	12	5	5										0.39
66075	T	3.4	—	—	123	92	75	59	52	43	37	34	25	23	19	15	14					0.59
66075	S	3.4	—	—	—	144	126	105	94	74	67	59	45	44	36	32	30	20	20	18		1.18
66075	N	3.4	—	—	—	213	205	189	174	152	139	131	99	93	81	73	68	52	51	48	47	45	2.75
66075	E	3.4	—	—	—	116	103	94	87	78	66	48	44	36	34	32	20	20	19	18		1.18
66075	W	3.4	—	—	—	53	50	45	41	38	34	34	30	30	27	25						0.78
68415	S	3.9	—	41	31	19	15	9														0.20
68415	N	3.9	—	89	63	37	26	21	12													0.39
69935	T	3.3	—	299	194	122	83	64	49													0.79
69935	T_F	3.3	127	80	37	24	15	11	6	3	—	1										0.52

			Counts at various Magnifications															
			50	100	150	200	300	350	400	450	500	550	600	700	800	900	100[b]	
60335	T[d]	3.0	67	64	50	45	29	24	17	15	8	1	1	1	1	1	1	3.14
61175	T[d]	3.0	—	97		84		70		50		40		34	23	20	17	9	3.14
69935	T[d]	3.3	852	702		279		98		45		30		18	13	6	2	1	4.89

[a]Average for entire rock (= A).
[b]Pit diameter (μm).
[c]Surface area per magnification and individual rock surface.
[d]Repeated counts by different observer (*see* Fig. 6).

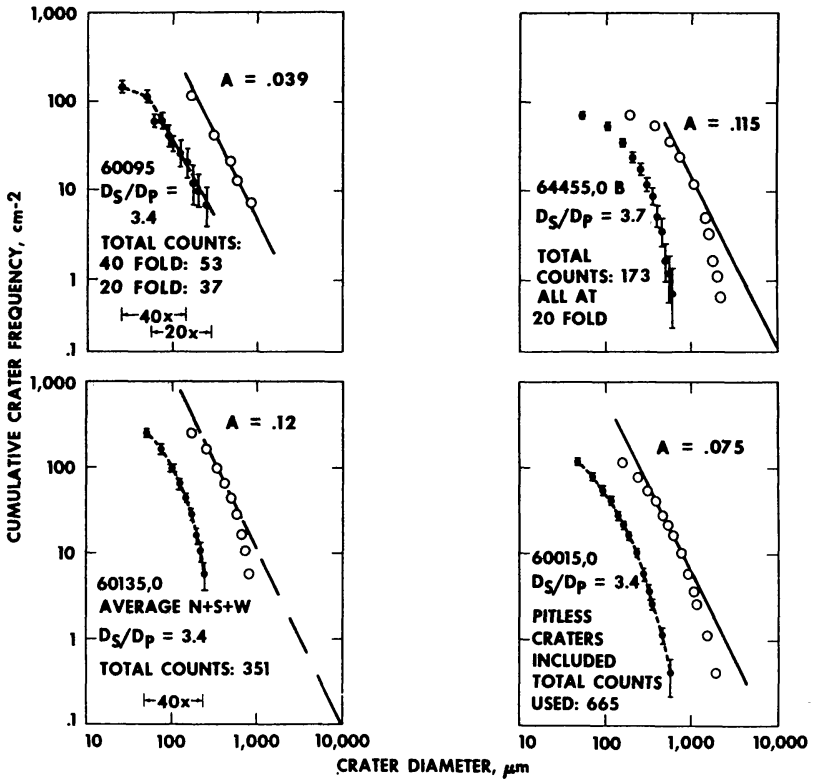

Fig. 1. Cumulative size frequency distributions of crater populations typical of Apollo 16 glass-surfaces in the production state. Dots represent the actual pit diameters measured; open circles represent the size-frequency distributions of the corresponding spall diameters as calculated from the measured D_S/S_P values. The best fit of a -2 slope through the spall diameters was graphically constructed to obtain the "areal density coefficient" (A), which is a numerical measure of the absolute number of craters per unit area. The following figures are constructed in identical fashion.

Smooth glass surfaces are by far the most suitable materials on which to observe such production conditions. We complemented our previous data with additional counts on rocks 60015, 60095, 60135, and 64455. These counts are illustrated in Fig. 1. Because of its large size, specimen 60015 was well suited for obtaining statistically significant data for pit diameters up to 625 μm. Production populations were also found on crystalline rocks, particularly on various surfaces of rock 61156 (N, E, T, S), as illustrated in Fig. 2. An additional production surface (Fig. 3) on breccia 69935 was investigated (T_F, indicating a freshly fractured area within the large surface, T).

The production distributions on Apollo 16 samples show a behavior similar to that seen earlier on Apollo 12 and 14 rocks (Bloch *et al.*, 1971; Hörz *et al.*, 1971; Hartung *et al.*, 1972; Neukum *et al.*, 1972; Morrison *et al.*, 1972). Figure 7 summarizes in a normalized way the statistically most significant production size distributions obtained to date on lunar glass surfaces. The slope of the log–log size distribution curve is about -2 at a pit diameter of 100 μm to 200 μm and steepens to -3 at a pit diameter of about 300 μm. The slope flattens to values of -1.0 to -1.5 at a pit diameter less than 100 μm.

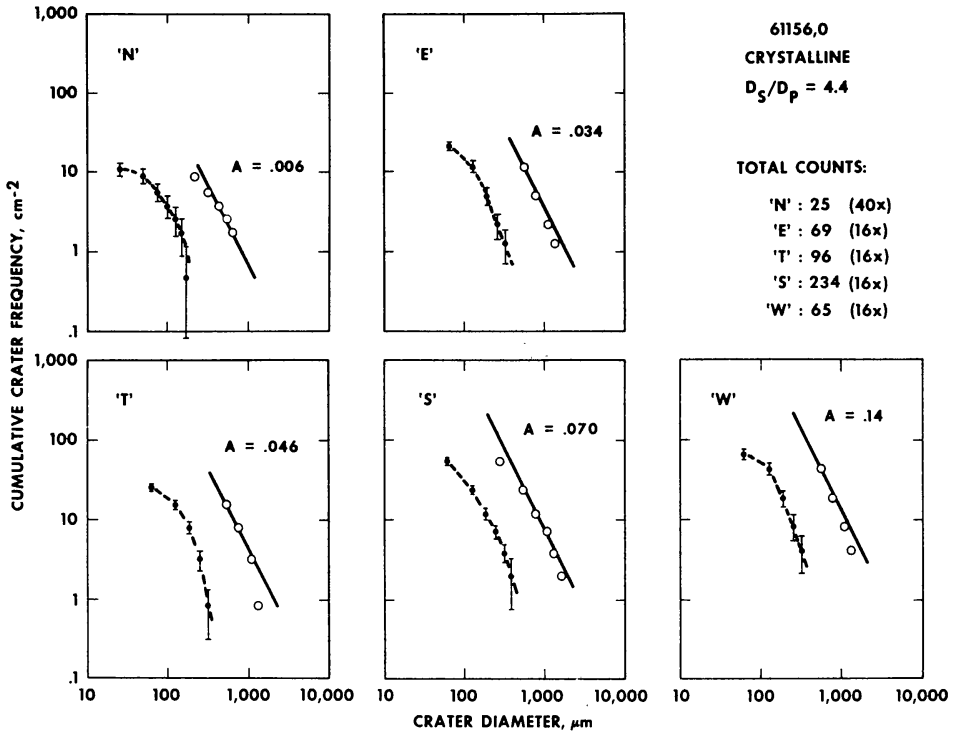

Fig. 2. Cumulative size frequency distribution of microcraters obtained on various sides of rock 61156,0. Note the various areal density coefficients for different surfaces. Surfaces N, E, T, and S are typical of production populations on crystalline rocks. The quality of the statistical data suffers from the small size of specimen 61156,0.

Despite the general similarity of the curves shown for different rocks, there are some subtle differences, which may be significant for the interpretation of the micrometeoroid complex. For example, sample 60135 shows a significantly steeper distribution than does rock 60015. Though this difference may be due to observational effects, it may also be attributed to different average impact angles which correspond to various solid angles of exposure. This effect may be understood analytically by considering a size distribution having a variable log–log slope. A straight-line size distribution at a given time may be represented as follows (Gault, 1970; Neukum and Dietzel, 1971), assuming a vertical impact angle,

$$N(D) = \frac{a\beta}{\alpha} k^{\alpha} D^{-\alpha}$$

where $N(D)$ is the cumulative number of craters greater than diameter D; a, β, and k are distribution and scaling constants; and α is the slope of the log–log crater size distribution. Based on laboratory experiments which take into account variable impact angles (Gault, 1973), the above equation may be modified to

$$N(D) = \frac{\alpha\beta}{\alpha} k^{\alpha} D^{-\alpha} (\sin i)^{\epsilon\alpha}$$

where i is the average impact angle, and ϵ is an empirical constant. A curved

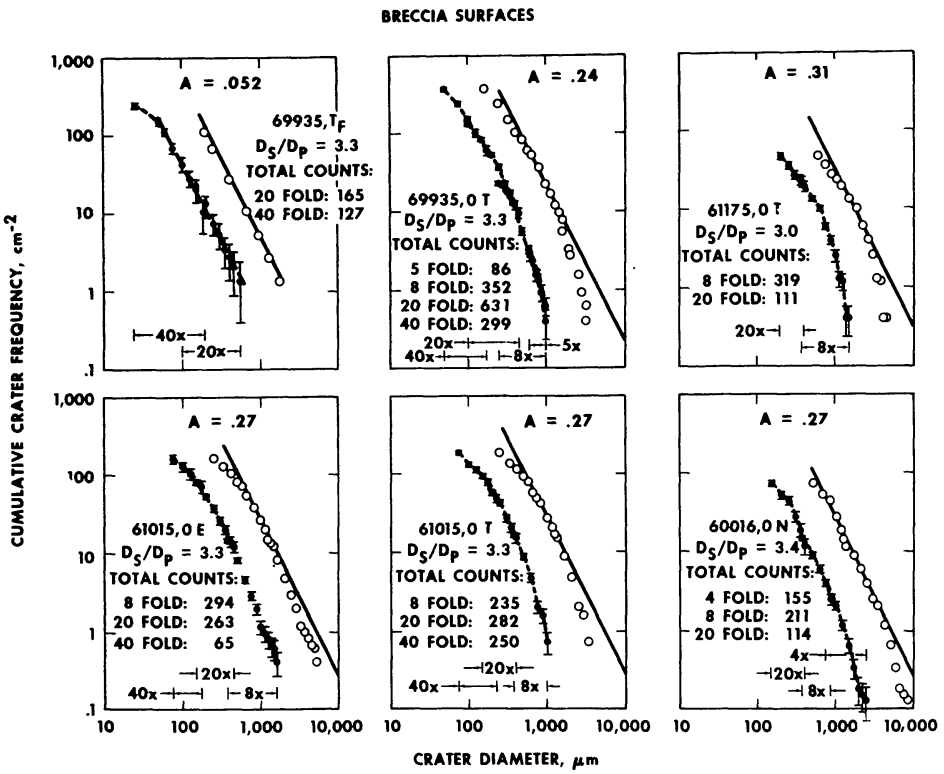

Fig. 3. Cumulative size frequency distributions of microcraters obtained on various Apollo 16 breccias. Note the difference in areal density for surfaces 69935,0 T, and 69935,0 T_F, the latter one being a typical production surface. Also note the identical areal density coefficients for surfaces 61015,0 E and 61015,0 T.

distribution may be represented by allowing α to be a variable, namely $\alpha = \alpha(D)$. For two diameters, D_1 and D_2, and an impact angle, i_1, we get

$$N_1(i_1) = \frac{a\beta}{\alpha_1} k^{\alpha_1} D_1^{-\alpha_1} (\sin i_1)^{\epsilon\alpha_1}$$

and

$$N_2(i_1) = \frac{a\beta}{\alpha_2} k^{\alpha_2} D_2^{-\alpha_2} (\sin i_1)^{\epsilon\alpha_2}$$

For an impact angle i_2, we get the analogous expressions, i_1 being replaced by i_2. For a *constant* shape of the distribution the following relationships must be valid.

$$\frac{N_1(i_1)}{N_1(i_2)} = \frac{N_2(i_1)}{N_2(i_2)}$$

and from above

$$\left(\frac{\sin i_1}{\sin i_2}\right)^{\epsilon\alpha_1} = \left(\frac{\sin i_1}{\sin i_2}\right)^{\epsilon\alpha_2}$$

which is true only when $i_1 = i_2$ or $\alpha_1 = \alpha_2$.

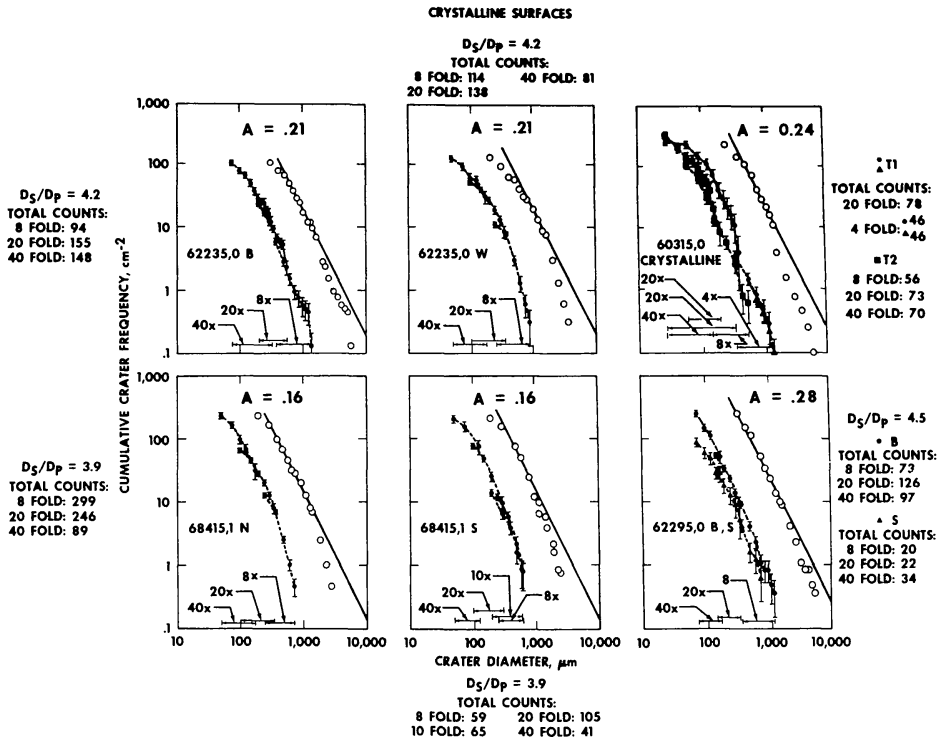

Fig. 4. Cumulative size frequency distributions of microcraters obtained on various Apollo 16 crystalline rocks. Note the identical areal density coefficients for various surfaces of rock 68415 (N, S) and 62235 (B, W) as well as the differences between 62235 B and S.

However, the slope, α, has been shown not to be constant, and we have postulated different average angles of impact, *i*. Therefore, the above relationships are not valid under these conditions. As a consequence, different impact angles in a size range where the production distribution slope is changing causes different shapes of the observed crater size distribution. For an assumed difference in $\sin i_1/\sin i_2$ of 1.4 (e.g., $i_1 = 45°$, $i_2 = 30°$) over the range of pit diameters from 50 to 500 μm, corresponding to slopes from about -1 to -3, a difference of a factor of 2 craters may be expected at one extreme of the distribution normalized at the other extreme.

Another somewhat more speculative prospect is that if interplanetary dust motion is confined to some degree to the ecliptic plane, then the shape of the size distribution of pits in this size range may be dependent upon the selenographic direction which the surface under study was facing. Unfortunately, however, such data are not available at present for the rocks investigated.

Equilibrium populations

After a sufficiently long exposure time, pre-existing craters on a surface will be destroyed by subsequent impacts. It is suggested that the cumulative crater density, $N(D)$, will change with time as shown qualitatively in Fig. 8. After some time the number of craters observed will be less than the extrapolated production

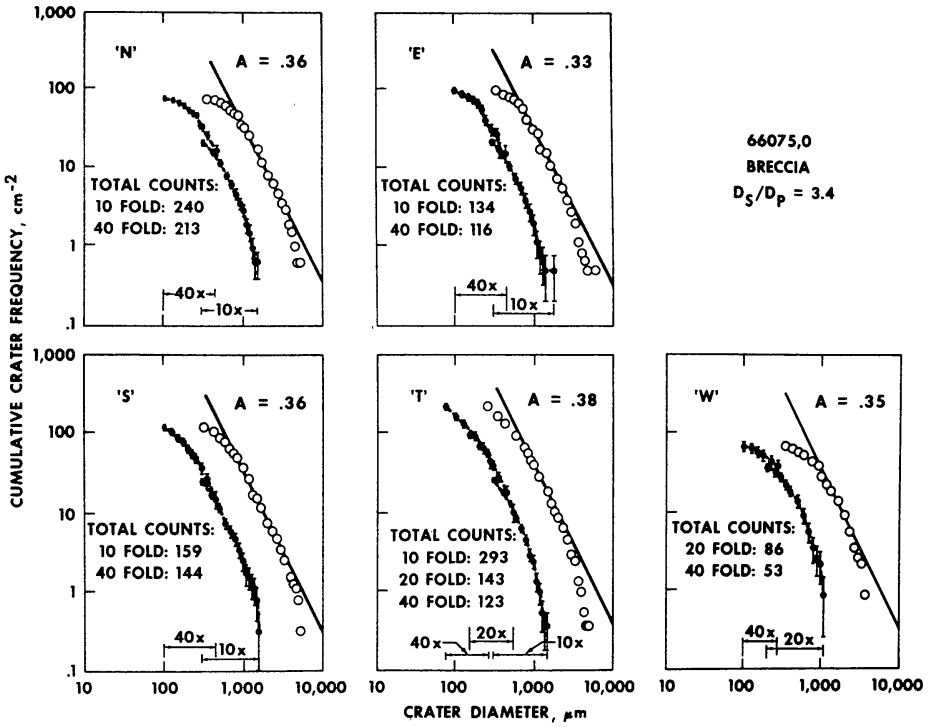

Fig. 5. Cumulative size frequency distributions of microcraters obtained on various surfaces of breccia 66075,0. Note the essentially identical areal density coefficients on all five surfaces.

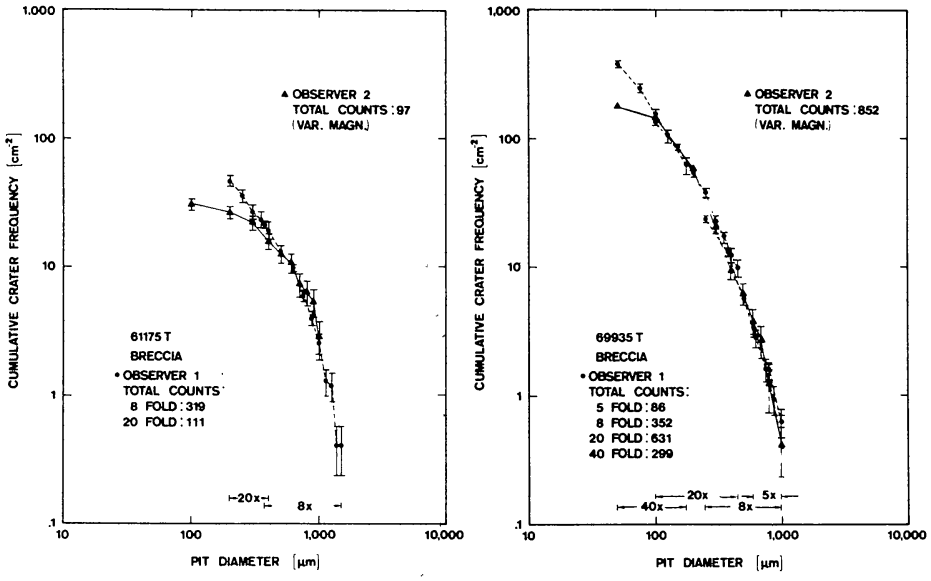

Fig. 6. Representative examples of cumulative size frequency distributions obtained by different observers on identical surfaces. The agreement is normally within 20%, except for the smallest sizes.

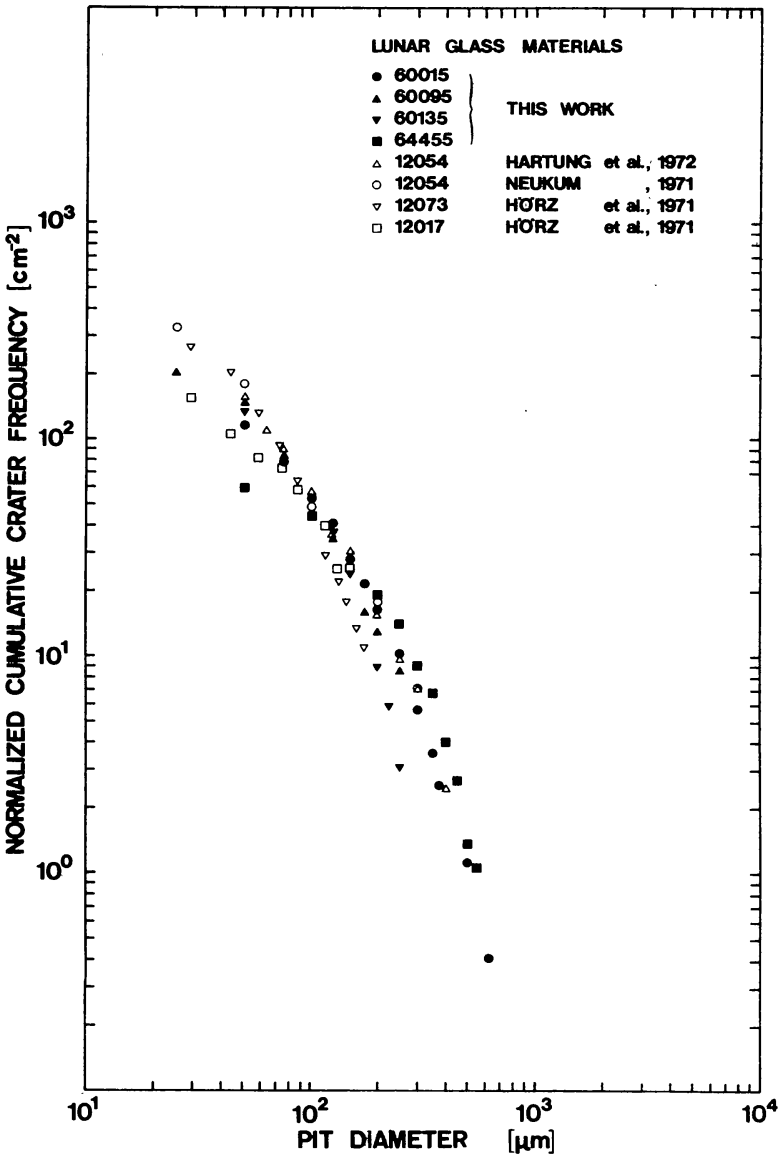

Fig. 7. Cumulative frequencies of microcraters obtained on a variety of glass-surfaces representing production populations for microcraters with pit diameters >25 μm. The consistent data for 12054 and 60015 are considered to be the most reliable because of the large number of craters counted in both cases. Note the relative steepening of the production slope at about 200 μm pit diameter resulting in a production slope steeper than -2. The curves are normalized at a pit diameter of 100 μm.

number. The population density gradually approaches an upper limit, $N_E(D)$, after passing through some intermediate transition stage. The boundaries between production, transition, and equilibrium are somewhat arbitrary, which is indicated by the overlapping ranges in the figure. In practice, however, a production state can usually be recognized visually because one can observe the failure of craters to overlap one another.

It is important at this point to establish criteria to be used as a basis for recognizing equilibrium crater populations. In the following sections we will

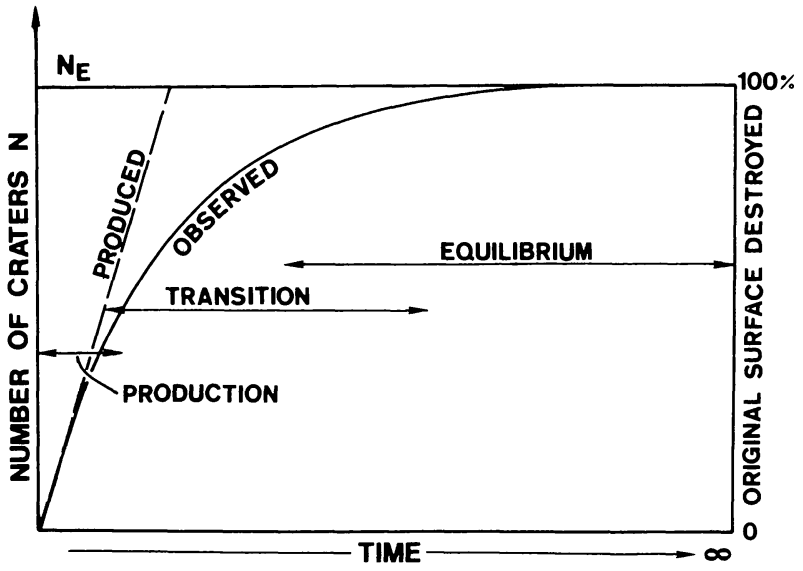

Fig. 8. Schematic development of a crater population where the only destruction mechanism operating is that of crater superposition. Note the gradual transition between production, transition, and equilibrium populations.

discuss four independent approaches toward establishing a particular crater size distribution as an equilibrium distribution.

1. *Absolute crater densities.* An analytical model has been developed which may be used to predict the crater density expected for equilibrium distributions. Hörz *et al.* (1971) pointed out that microcraters on hard lunar rocks are exclusively destroyed by direct superposition of subsequent impacts. Ballistic sedimentation can be neglected, though it is the dominant process of crater obliteration on the loose, lunar regolith surface according to Gault (1970), Soderblom (1970), and others. Consequently, models of the development of crater populations neglecting ballistic sedimentation (Marcus, 1964, 1966, 1970; Walker, 1967; Chapman *et al.*, 1968; Neukum and Dietzel, 1971) are better suited to describe the development of microcrater populations on hard lunar rocks over geologic periods of time. Based on these models the cumulative equilibrium density, $N_E(D)$, is a well-defined quantity and can be derived from the general expression for destruction by superposition as time approaches infinity. The expression from Neukum and Dietzel (1971) reads $N_E(2(\alpha-2))/(\pi \cdot b^{(2-\alpha)/\beta}) \times D^{-2}$, where D can be either D_P or D_S. The quantity b can be defined by the relation $m_{\min} = bm$ which in terms of crater diameter gives $D_{\min} = b^{1/\beta} \times D$. D represents the diameter of the target crater and $D_{\min}$ is the diameter of the crater formed by $m_{\min}$ able to destroy the target crater. The above formula gives a general expression for the crater size distribution in equilibrium for a constant $\alpha > 2$. The case $\alpha < 2$ is not considered here. Therefore, the concept, as defined above, may be applied only to craters with pit diameter >250 μm. In addition, the expression derived for the equilibrium crater density is valid in this form only for an infinite distribution ($m_{\max} \to \infty$). Because we have finite distributions on lunar rocks, i.e., the largest crater has a diameter,

$D_{max} < \infty$, the relation will be approximately correct for a limited size range. This limited range we call the "D^{-2} range of equilibrium". For an idealized representation of the relationships discussed, see Fig. 9. The end of the equilibrium distribution corresponding to large craters may be close to the production state because impact events are not frequent enough to destroy the large craters in this range. The opposite end of the equilibrium distribution reflects the flattening of the production distribution at smaller sizes.

To establish the criteria for destruction of an existing crater by a later impact, we set

$$b^{1/\beta} = \frac{D_S}{D_P}$$

This means an impact event with a spall diameter the same size as the pit diameter of the target crater will destroy the target crater. This is a conservative assumption in the sense that it would probably require a larger impact event to destroy the target crater. Thus, the minimum equilibrium crater size distribution for a lunar rock surface where only pit diameters can be quantitatively recorded may be written,

$$N_E = \frac{2(\alpha - 2)}{\pi} \left(\frac{D_P}{D_S}\right)^{\alpha - 2} D_S^{-2}$$

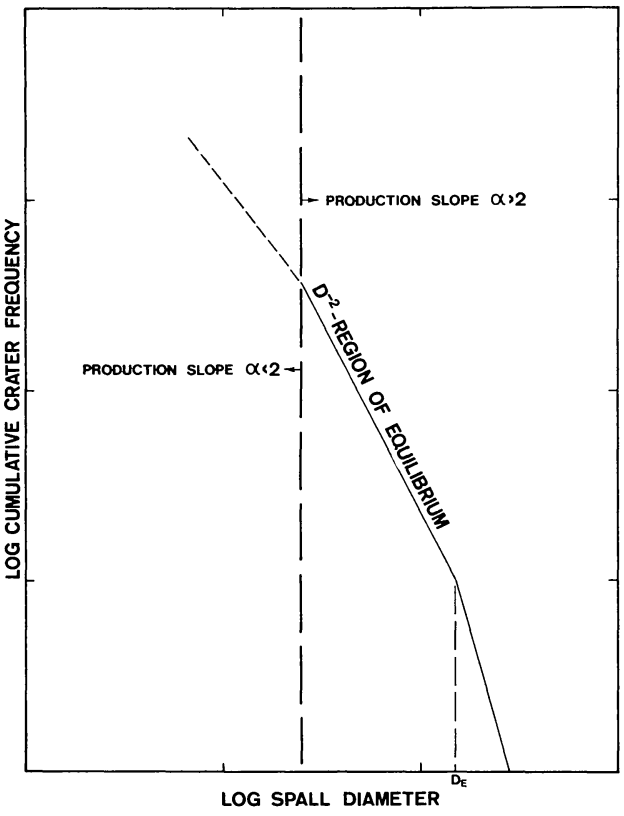

Fig. 9. Schematic of a lunar rock crater size frequency distribution in the equilibrium state.

In order to compare the crater densities obtained using this analytical expression with measured densities from various rocks, we define a standard quantity as follows by simplifying the above relationship:

$$N_E = A\, D_S^{-2}$$

where A is the equilibrium areal crater density coefficient, or simply areal density coefficient, and is given by

$$A = \frac{2(\alpha-2)}{\pi}\left(\frac{D_P}{D_S}\right)^{\alpha-2}$$

On rocks with different D_S/D_P ratios we must expect different values of A. The D_S/D_P ratio on one rock may furthermore vary with exposure time because of increasing degree of microfracturing of surface materials. Thus the areal density coefficient varies not only from rock to rock but it may also vary for one given specimen even though an equilibrium state, i.e., an extended D^{-2}-region of equilibrium, was reached earlier.

The absolute value of A for a given D_P/D_S is dependent on the production slope, α. Thus, for numerical calculations it must be known. In reality the slope, α, is not quite constant in the range, $D_P > 250\ \mu$m. However, a variation from $\alpha = 2.7$ to $\alpha = 3.5$ will not significantly influence the areal density coefficient, A. For D_S/D_P ratios between 2.7 and 4.5 we have a variation in A by $\lesssim 20\%$. Thus, within the limits of the accuracy of our measurements, we can treat the problem as if we deal with a constant slope, $\alpha = 3$.

The analytically derived values of $A(A_{\text{anal.}})$ based on an α of 3.0 and an average of measured values of D_P/D_S for a given rock, may be compared with measured values of $A(A_{\text{meas.}})$. This quantity was determined by drawing a line of -2 slope through the distributions on the log–log plot and reading $A_{\text{meas.}}$ on the cumulative number scale where the line intersected the crater-diameter coordinate at $D_S =$ 1 cm. These lines and the corresponding equilibrium areal crater density coefficients, or areal density coefficients, are also shown on Figs. 1 through 5. Although A is defined in terms of an equilibrium distribution having a -2 slope, it may also be applied as a measure of production or transition distributions which have a -2 slope. For the greatest measured value $D_S/D_P = 4.5$ (crystalline rocks) the analytical model gives a value of $A_{\text{anal.}} = 0.15$. This is the minimum equilibrium areal density coefficient to be expected for crater populations in equilibrium on lunar rocks, if no larger D_S/D_P ratio occurs.

The comparison between analytically derived and measured densities for Apollo 12, 14, and 16 rocks is shown in Table 3. Agreement is fair, however, in a few cases, especially for breccias, there is considerable deviation. With the quality of the observational data in mind, we may classify surfaces with $A_{\text{meas.}}/A_{\text{anal.}}$ in the range 0.7–1 as probably not being in equilibrium and surfaces with values between 1 and 1.5 as being in equilibrium. In some cases $A_{\text{meas.}}/A_{\text{anal.}}$ exceeds 1.5. For these, and perhaps other cases, we suggest that the surfaces are in equilibrium and the effective destruction diameter for a given cratering event may be less than D_S.

Such a case is indicated by the close proximity of two glass-lined pits shown in

Table 3. Comparison of measured and calculated maximum areal density coefficients on Apollo 12, 14, and 16 rocks.

Rock	D_S/D_P	$A_{meas.}$	$A_{anal.}$	$\frac{A_{meas.}}{A_{anal.}}$
"Crystalline"				
12006 (III)	4.5*	0.12	0.15	0.8
12017 (I)	4.5*	0.12	0.15	0.8
12021 (II)	4.5*	0.11	0.15	0.7
12038 (II)	4.5*	0.19	0.15	1.3
12047 (I)	4.5*	0.12	0.15	0.8
12051 (I)	4.5*	0.13	0.15	0.9
12053,37	4.5*	0.17	0.15	1.1
12063,106	4.5*	0.18	0.15	1.2
14053	3.6	0.13	0.18	0.7
60315 T	3.7	0.24	0.18	1.3
61156 W	4.4	0.14	0.15	0.9
62235 B	4.2	0.21	0.16	1.3
62235 W	4.2	0.21	0.16	1.3
62295 B	4.5	0.28	0.15	1.9
68415,1N	3.9	0.16	0.17	0.9
68415,1S	3.9	0.16	0.17	0.9
"Breccia"				
12073	4.5	0.18	0.15	1.2
14303,13	3.4†	0.21	0.20	1.1
14305, (D_3)	3.5	0.44	0.19	2.3
14306 (1)	3.4	0.64	0.20	3.2
14318 (B_2)	3.5	0.39	0.19	2.1
14321 (I)	4.5	0.40	0.15	2.7
60016 N	3.4	0.27	0.20	1.4
61015 T	3.3	0.27	0.20	1.4
61015 E	3.3	0.27	0.20	1.4
61175 T	3.0	0.31	0.22	1.4
66075 T	3.4	0.38	0.20	1.9
66075 S	3.4	0.36	0.20	1.8
66075 N	3.4	0.36	0.20	1.8
66075 E	3.4	0.33	0.20	1.7
66075 W	3.4	0.35	0.20	1.8
69935 T	3.3	0.24	0.20	1.2

*Average for all Apollo 12 crystalline rocks.
†Not determined; typical value for breccias.

the photograph and the idealized sketch in Fig. 10. One might expect that the spall zone of the more recent event would have destroyed a nearby older pit. Thus, there appears to be another unknown parameter which governs the ease with which a rock retains central glass pits. The parameters causing such an apparent decrease in the effective destruction radius are unknown at present. Therefore, our model, which assumes the measured D_S is the diameter of destruction, cannot be expected to explain all effects and give exact values for equilibrium crater densities on different types of rocks.

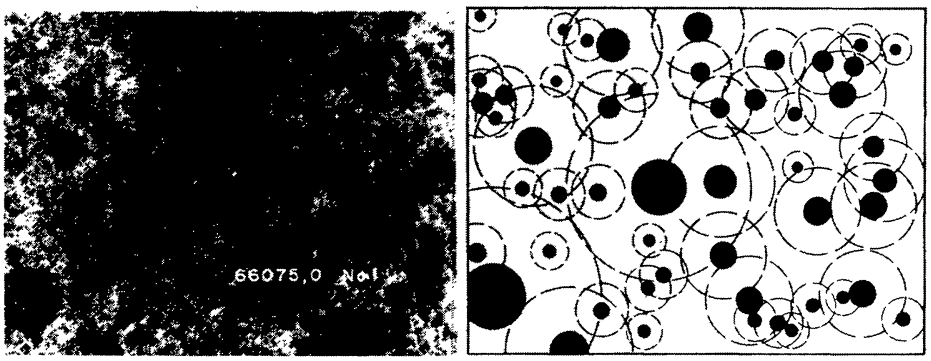

Fig. 10. Close-up photograph of rock 66075,0 considered to represent an equilibrium population. (Width of frame approximately 1 cm.) For comparison a sketch depicting actual central pit locations and size (black dots) is added and the actual, as well as eroded, spall zones (dashed circles) are indicated using the measured D_S/D_P value. Note the close proximity of many events demonstrating that the effective destruction diameter operating in this surface is D_S. Note also the relative paucity of small events within the (somewhat younger) spall zone of the big crater in the center.

2. *Constant crater density for different exposure angles.* If the absolute crater densities on different surfaces of the same rock are different from one another, one must postulate—based on exposure geometry arguments—that only the crater population with the highest density observed can potentially correspond to equilibrium. It may, of course, still be in the transition state while crater populations with the lower densities must either be in the production or transition state. Examples of varying crater densities for individual faces are rocks 61156 (surfaces N,E,T,S,W), 62295 (surfaces B,S) and 60315 (surfaces T_1 and T_2).

If, however, a well documented rock displays identical crater densities on surfaces of drastically different exposure geometries, the following conclusions may be drawn: the surface with the optimum solid angle of exposure must always display more craters than all the other surfaces; only after it reaches "equilibrium" will the number of craters remain constant. However, during this period, surfaces of less favorable exposure geometries will still accumulate more craters until they also finally reach equilibrium. This stage is indicated when all surfaces have the same crater densities. We suggest that the following rocks belong to this category: 62235 (surfaces T and W), and 66075 (surfaces T,S,N,E,W). These criteria are, of course, valid only if one can demonstrate that such rocks did not tumble repeatedly, i.e., that they possess at least one surface which is not cratered at all. As indicated earlier, the uncertainty associated with the crater densities may be as high as 50%, though as a general rule they can be judged to be better than 20%. Nevertheless, the lack of better accuracy may result in ambiguous interpretations.

3. *Extent of D^{-2} slope.* As an additional criterion, the extent of the D^{-2} slope may be considered to establish "equilibrium" conditions. The more the D^{-2} slope deviates from production distributions, by extending to spall zone diameters significantly greater than 1000 μm, the more likely it is that such surfaces are in

equilibrium. Surfaces of this category are: 60016 N, 61175 T, 61015 T and E, and 66075 T, N, E, S, W. Here again, however, unambiguous interpretations are limited by the quality of statistical data available, especially at larger crater sizes.

4. *Erosional state of surface.* Another criterion is based on the optical inspection of a given rock surface for either evidence of abundant overlap of cratering events or the presence of original uncratered rock surface. If the cratered surfaces of a given rock differ drastically in their degree of roundness with the uncratered surfaces, it may be concluded that mass-wasting has proceeded so far that no original rock-surface has been preserved. Thus, well rounded surfaces may possess "equilibrium" crater populations. Surfaces of this category are: 60315 T_1, 62235 B and W, 62295 B, 60016 N, 61175 T, 61015 E and T, 68415 N and S, and 66075 T, N, E, S, W.

In Table 4 the observational data are compared with these four criteria for equilibrium. The only surfaces which qualify in all aspects are 62235 B, W and 66075 T, N, E, S, W. All other surfaces remain ambiguous in their interpretation.

Comparison of Crater Densities

Maximum measured areal density coefficients for a number of different rocks with different physical properties are plotted in Fig. 11 together with the limiting frequency value of Morrison *et al.* (1972). Gault's (1970) saturation percent values are given for comparison with the areal density coefficient values. We find, especially for the Apollo 16 rocks, a wide range of crater densities. Low maximum values for "glass" surfaces occur because we measured essentially populations in the

Table 4. Evaluation of various criteria to establish equilibrium conditions on densely cratered Apollo 16 rocks.

Criterion		1	2			3	4	
Rock	Locations	$\frac{A_{meas.}}{A_{anal.}}$ (>1)	Exposure History Simple (no tumbling)	Geometry Different	Equal A	Extended D^{-2} Region	Rounded Surface	Equilibrium
60016	N	×		—	—	×	×	likely
60315	T_1, T_2	×	×	×	—	×(T_1)	×	T_1: doubtful, T_2: no
61015	T, E	×	?	?	×	×	×	likely
61175	T	×	—	—	—	×	×	likely
62235	B, W	×	×	×	×	×	×	yes
62295	B, S	×	×	×	—	×(B)	×	B: doubtful S: no
66075	T,N,E,S,W	×	×	×	×	×	×	yes
68415	N, S	×	×	?	×	×	×	doubtful
69935	T	×	×	—	—	×	?	doubtful

× indicates criterion for equilibrium satisfied.

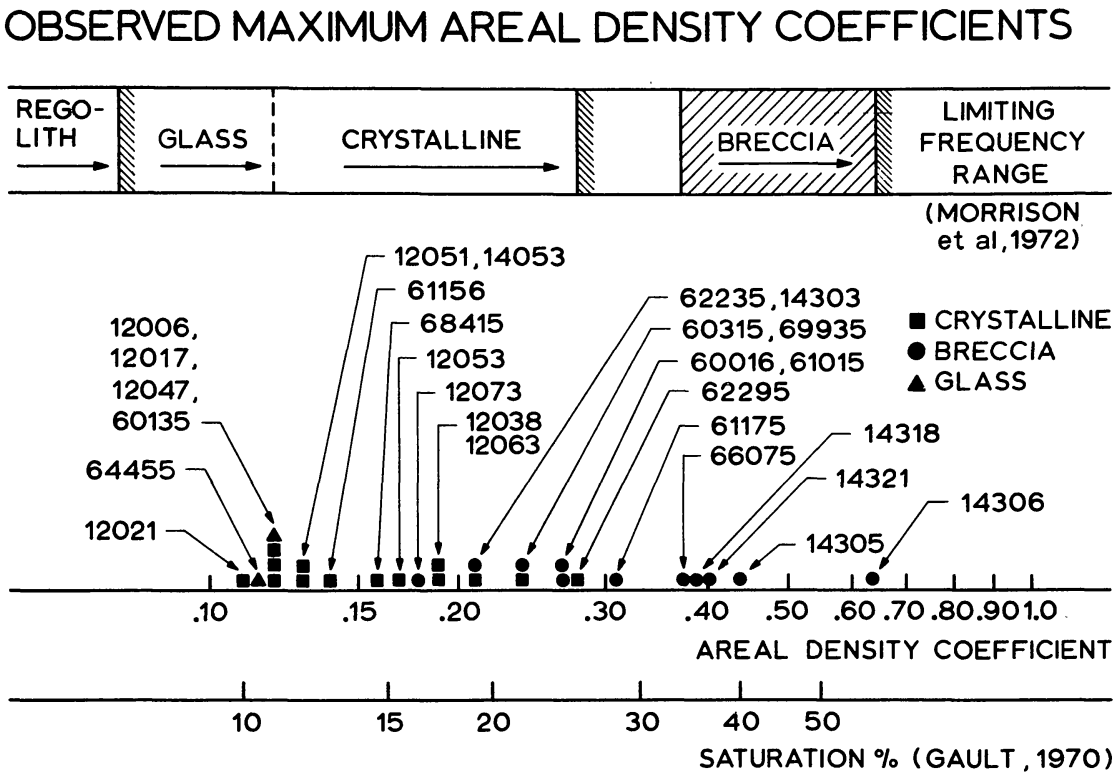

Fig. 11. Comparison of highest areal density coefficients observed to date on various lunar surface materials. Only the highest densities are plotted. Note the systematic difference of the areal density coefficients for various lunar rocks. These differences may be attributed to exposure age, rock properties, or a combination of both. The areal density coefficients for glass do not necessarily mean the highest approachable densities because only production populations have been investigated. For comparison, coefficients for loose regolith are indicated. Also shown are saturation percent values defined by Gault (1970).

production state. Other populations with similar values may be considered also in production provided D_S/D_P is the same. Regarding the higher areal density values we have concluded that these populations are in or approaching the equilibrium state. We find no simple relationship between areal density values for populations close to equilibrium and physical properties of the rocks. For example, rocks 60016 and 61175 are polymict breccias with only moderate intergranular coherency (PET), whereas 62295 is a crystalline rock (metaclastic) with tough intergranular coherency (PET), but the crater density coefficients are nearly the same. Similarly 68415 and 61156 are "crystalline" rocks very similar to 62295 in terms of intergranular coherence but their crater density coefficients are much lower than 62295. In general, however, crystalline rocks seem to have lower maximum densities than breccias.

None of the areal densities exceeds the limiting frequency range of Morrison *et al.* (1972); but all are greater than densities observed for the lunar regolith (Shoemaker *et al.*, 1970; Soderblom, 1970; Oberbeck and Quaide, 1968) and for cratering experiments in loose sand (Gault, 1970) (denoted "Regolith" in Fig. 11).

These low densities in loose materials are explained by the fact that erosion and ballistic sedimentation are the most effective mechanisms for crater obliteration in such target materials. The higher density of craters on lunar rocks demonstrates that microcraters are destroyed by the superposition of individual events.

Conclusions

Crater populations evolve in terms of cumulative size frequency distributions starting with the production state and reach equilibrium crater densities at larger crater size after passing through a transition stage.

Counts on four glass surfaces have yielded reliable statistics for production size distributions. Some differences in the shape of the distributions observed may be due to different exposure geometry of the surfaces studied.

Four criteria to distinguish between production and equilibrium cumulative crater size frequencies are: (1) absolute crater densities, (2) a constant crater density for surfaces of varying exposure geometry on the same rock suggest that equilibrium has been achieved, (3) an extended -2 slope for the cumulative crater frequency distribution particularly at the largest crater diameters measured, suggests equilibrium, (4) the erosional state of a surface, i.e., evidence for extensive rounding and mass removal may indicate equilibrium. Only populations from two rocks satisfied all four criteria and were unambiguously shown to be in an equilibrium state.

Our results confirm that destruction by superposition is the dominant process for crater obliteration on lunar rocks. The application of the analytical model yields for the cumulative equilibrium crater density, $N_E = A \cdot D_S^{-2}$. For spall-to-pit diameter ratios no greater than 4.5 there exists a minimum areal density coefficient $A = 0.15$ (equivalent to 14% saturation) for populations in equilibrium. This is consistent with our measurements.

The wide range of areal density coefficients in excess of the theoretical lower limit is at present not fully understood. These differences may be attributed to exposure age, rock properties, or a combination of both. These different views require separate discussions.

Acknowledgment—The research reported here was done while the first author was a Visiting Scientist at the Lunar Science Institute, which is operated by USRA under NASA contract NSR 09-051-001. This paper constitutes Lunar Science Institute Contribution No. 150.

References

Bloch M. R., Fechtig H., Gentner W., Neukum G., and Schneider E. (1971a) Meteorite impact craters, crater simulations, and the meteoroid flux in the early solar system. *Proc. Second Lunar Sci. Conf., Geochim. Cosmochim. Acta,* Suppl. 2, Vol. 3, pp. 2639–2652. MIT Press.

Chapman C. R., Pollack J. B., and Sagan C. (1968) An analysis of the Mariner 4 photography of Mars. *Smithsonian Astrophys. Observ. Spec. Rep.* **268**.

Gault D. E. (1970) Saturation and equilibrium conditions for impact cratering on the lunar surface: Criteria and implications. *Radio Sci.* **5**, 273–291.

Gault D. E. (1973) Displaced mass, depth, diameter, and effects of oblique trajectories for impact craters formed in dense crystalline rocks. *The Moon* **6**, 32–44.

Gault D. E., Hörz F., and Hartung J. B. (1972) Effects of microcratering on the lunar surface. *Proc. Third Lunar Sci. Conf., Geochim. Cosmochim. Acta*, Suppl. 3, Vol. 3, pp. 2713–2734. MIT Press.

Hartung J. B., Hörz F., and Gault D. E. (1972) Lunar microcraters and interplanetary dust. *Proc. Third Lunar Sci. Conf., Geochim. Cosmochim. Acta*, Suppl. 3, Vol. 3, pp. 2735–2753. MIT Press.

Hörz F., Hartung J. B., and Gault D. E. (1971) Micrometeorite craters on lunar rock surfaces. *J. Geophys. Res.* **76**, 5770–5798.

Hörz F., Carrier W. D., Young J. W., Duke C. M., Nagle J. G., and Fryxell R. (1972) Apollo 16 special samples. NASA-SP. In press.

Lunar Sample Preliminary Examination Team (1972) The Apollo 16 lunar samples: Petrographic and chemical description. *Science* **179**, 23–34.

Marcus A. H. (1964) A stochastic model of the formation and survival of lunar craters, 1. *Icarus* **3**, 460–472.

Marcus A. H. (1966) A stochastic model of the formation and survival of lunar craters, 2. *Icarus* **5**, 165–177.

Marcus A. H. (1970) Comparison of equilibrium size distributions for lunar craters. *J. Geophys. Res.* **75**, 4977–4984.

McKay D. S. (1970) Microcraters in lunar samples. *Proc. 28th Annual Mtg. Electron Microsc. Soc. Amer.* (editor C. J. Arceneaux), pp. 22–23. Claitors.

Morrison D. A., McKay D. S., Moore H. J., and Heiken G. H. (1972) Microcraters on lunar rocks. *Proc. Third Lunar Sci. Conf., Geochim. Cosmochim. Acta*, Suppl. 3, Vol. 3, pp. 2767–2791. MIT Press.

Neukum G. (1971) Untersuchungen über Einschlagskrater auf dem Mond. Doctor's thesis, University of Heidelberg.

Neukum G. and Dietzel H. (1971) On the development of the crater population on the moon with time under meteoroid and solar wind bombardment. *Earth Planet. Sci. Lett.* **12**, 59–66.

Neukum G., Schneider E., Mehl A., Storzer D., Wagner G. A., Fechtig H., and Bloch M. R. (1972) Lunar craters and exposure ages derived from crater statistics and solar flare tracks. *Proc. Third Lunar Sci. Conf., Geochim. Cosmochim. Acta*, Suppl. 3, Vol. 3, pp. 2793–2810. MIT Press.

Oberbeck V. R. and Quaide W. L. (1968) Genetic implications of lunar regolith thickness variations. *Icarus* **9**, 446–465.

Schneider E., Storzer D., and Fechtig H. (1972) Exposure ages of Apollo 15 samples by means of microcrater statistics and solar flare particle tracks. In *The Apollo 15 Lunar Samples*, pp. 415–419, The Lunar Science Institute, Houston.

Shoemaker E. M., Batson R. M., Holt H. E., Morris E. C., Rennilson J. J., and Whitaker E. A. (1969) Observations of the lunar regolith and the earth from the television camera on Surveyor 7. *J. Geophys. Res.* **74**, 6081–6119.

Shoemaker E. M., Hait M. H., Swann G. A., Schleicher D. L., Schaber R. L., Sutton R. L., Dahlem D. H., Goddard E. N., and Waters A. C. (1970) Origin of the lunar regolith of Tranquillity Base. *Proc. Apollo 11 Lunar Sci. Conf., Geochim. Cosmochim. Acta*, Suppl. 1, Vol. 3, pp. 2399–2412. Pergamon.

Soderblom L. A. (1970) A model for lunar impact erosion applied to the lunar surface. *J. Geophys. Res.* **75**, pp. 2655–2661.

Walker E. H. (1967) Statistics of impact crater accumulation on the lunar surface exposed to a distribution of impacting bodies. *Icarus* **7**, 233–243.